Nat Neurosci. Author manuscript; available in PMC 2018 February 19.

Published in final edited form as:

Nat Neurosci. 2016 February ; 19(2): 290–298. doi:10.1038/nn.4209.

Hypothalamic feed-forward inhibition of thalamocortical network controls arousal and consciousness

Carolina Gutierrez Herrera[1,2,4], **Marta Carus Cadavieco**[3], **Sonia Jego**[2], **Alexey Ponomarenko**[3], **Tatiana Korotkova**[3], and **Antoine Adamantidis**[1,2,4,*]

[1]Department of Neurology, Inselspital University Hospital, University of Bern, Bern, Switzerland [2]Douglas Mental Health University Institute, Department of Psychiatry, McGill University, Montreal, Canada [3]Leibniz Institute for Molecular Pharmacology (FMP)/NeuroCure Cluster of Excellence, Berlin, Germany [4]Department of Preclinical Research (DKF), University of Bern, Bern, Switzerland

Abstract

During non-rapid eye movement (NREM) sleep, synchronous synaptic activity within the thalamocortical network generates predominantly low frequency oscillations (< 4 Hz) that are modulated by inhibitory inputs from the thalamic reticular nucleus (TRN). Whether TRN cells integrate sleep-wake signals from sub-cortical circuits remains unclear. Here, we identified a monosynaptic LH_{GABA}-TRN_{GABA} transmission that exerts a strong inhibitory control over TRN neurons. We showed that optogenetic activation of this circuit recapitulated state-dependent changes of TRN neuron activity in behaving mice and induced rapid arousal during NREM, but not REM sleep. During deep anesthesia, activation of this circuit induced sustained cortical arousal. In contrast, optogenetic silencing of LH_{GABA}-TRN_{GABA} increased the duration of NREM sleep and amplitude of delta (1–4 Hz) oscillations. Collectively, these results demonstrate that TRN cells integrate subcortical arousal inputs selectively during NREM sleep and may participate in sleep intensity.

In mammals, during non-rapid eye movement (NREM) sleep, the electroencephalogram (EEG) activity shows typical signs of brain activity that include a predominant slow wave (< 1 Hz) associated with delta oscillations (1–4 Hz) and spindles (11–15 Hz) [1–3]. Slow wave oscillations reflect the slow variation of the resting membrane potential of cortical neurons that switches between depolarized ("UP") and a hyperpolarized ("DOWN") states [4]. During the UP state, thalamocortical (TC) and corticothalamic (CT) cells show intense synaptic activity and burst firing, while during the DOWN state their progressive hyperpolarization

*Correspondence should be addressed: Antoine Adamantidis, Ph.D., University of Bern, Dept of Neurology, Inselspital University Hospital, Freiburgstrasse, 18, 3010 Bern, Switzerland, Tel: +41 (0)31 632 55 93, antoine.adamantidis@dkf.unibe.ch.

Author contribution.

All authors designed the experiments. C.G.H. collected and analyzed anatomical, *in vitro* electrophysiological, behavioural/polysomnographic/optostimulation data. S.J. collected behavioural/polysomnographic/optostimulation preliminary data. M.C.C. and A.P. collected and M.C.C., A.P. and T.K. analyzed *in vivo* LH and TRN electrophysiological/optostimulation data. All authors discussed the results and C.G.H., M.C.C., A.P, T.K. and A.A. wrote the manuscript.

induces a period relative quiescence. Slow wave oscillations have a cortical origin [5] and, presumably, coordinate other sleep rhythms, including spindles and delta oscillations, into a coherent rhythmic sequence of cortico-thalamo-cortical rhythm [1,4,6].

Changes in thalamocortical cell firing are largely controlled by inhibitory TRN cells and correlate with spindles, delta waves and spike-wave discharge during epileptic seizures [1,7,8]. The TRN is a thin sheet of GABAergic cells encasing the thalamus where they exert a strong inhibition control over TC relay cells [9,10]. In turn, TRN neurons are activated by glutamatergic axon collaterals from TC and CT cells, providing a positive feedback onto TRN cells [1,7,11]. The activity of TRN cells is also directly modulated by extra-thalamic GABA inputs [12], sleep-wake neuromodulators/transmitters including acethycholine[13,14], norepinephrine[1] and peptides[15,16], as shown *in vitro* and *in silico*[17–19]. Inhibitory postsynaptic currents (IPSCs) have been recorded in TRN cells in brain slices[20–22], however, the origin of these inhibitory inputs remains unclear. In agreement with *in vitro* studies, direct activation of TRN cells during wakefulness produces profound alterations of thalamo-cortical network activity, including cortical gamma oscillations (~30–150 Hz)[23], spindles[24,25] and cortical slow-waves [25], that directly depend on the stimulation frequency and type (electrical *vs* optogenetic). Collectively, these results suggest that TRN cells integrate extra-thalamic signals related to sleep-wake control, and behavioral state transitions in particular.

Based on our recent mapping of sleep-wake circuits in the lateral hypothalamus (LH) [26,27], we hypothesized that changes in the activity of sub-cortical neurocircuits can directly modulate thalamocortical network activity, hence, exerting a direct control onto vigilance state-dependent oscillations. In this framework, g-aminobutyric acid (GABA)-producing cells in LH are a strong candidate since they are known to control a large repertoire of sleep and awake processing ranging from sleep to arousal, attention, reward and stress[28–32]. Here, we investigated the functional connectivity between the LH_{GABA} and TRN and its role in bottom-up control of thalamocortical oscillations during sleep using a combination of genetically-encoded optogenetic tools and *in vitro/vivo* electrophysiological methods.

Results

Activation of LH_{GABA} neurons induces rapid wakefulness

First, we investigated the role of LH_{GABA} neurons in sleep-wake control in light of their heterogeneous activity and discharge profile during those state [31]. Behavioral consequences of activation of LH_{GABA} neurons during sleep states were studied using optogenetics combined with electrophysiological recordings in freely-moving animals (See Methods). To genetically target GABA neurons in the LH area, we stereotactically injected a adeno-associated virus (AAV) carrying a Cre-inducible vector encoding either the light-activatable channelrhodopsin-2 variant ChETA in-frame fused to enhanced yellow fluorescent protein (ChETA-EYFP) or EYFP (control) in the LH of Tg(VGAT)::IRES-Cre transgenic mice (mice expressing the Cre recombinase in cells expressing the vesicular g-aminobutyric acid transporter (VGAT) gene[33]) (Fig. 1a).

Consistent with other studies [32,33], we found that this method allows selective targeting of LH_{GABA} neuron cell bodies (97.4 ± 0.5 % of GAD^+/YFP^+; 2.2 ± 0.5 % of YFP^+/GAD^- cells (N = 3 sections per animal, 12 animals, F (2, 42) = 99.89 $P = 0.0001$, repeted measures followed by Bonfferoni post-hoc test; Fig. 1a, b and Supplementary Fig. 1a–c) and their axons (Supplementary Fig. 1d). Our genetic targeting was restricted to LH area as shown by the limited expression of ChETA-YFP-expressing cell bodies in the zona incerta (ZI; dorsal to the LH) and other areas adjacent to the LH (Supplementary Fig. 1b). Genetic targeting of LH_{GABA} cells with ChETA-YFP allows optical control of their activity over a wide range of frequencies *in vitro* (1–50 Hz; Supplementary Fig. 2a–e). To test for a role of LH_{GABA} cells in sleep-wake control, transduced animals were chronically implanted with movable silicon probes in LH and bilateral optical fibers directly above LH for optogenetic activation of LH_{GABA} cell bodies and simultaneous electrophysiological and polysomnographic recordings (see Methods; Fig 1a and Supplementary Fig. 3a, b). We found that a population of LH cells ($N = 31$, 4 mice) increased their firing rate with a short latency (<10 ms) upon optical stimulation (Fig 1c–g; Supplementary Fig. 3c–d; for 1-s pulses: N=18, 1 mouse $t(17,17) = -2.359$, $P = 0.0306$, two-tailed t-test). These, photo-responsive, i.e. presumably ChETA-expressing LH_{GABA} cells, fired with mean firing rates of 4.42 ± 0.64 Hz and inter-spike intervals (ISI) of 459.69 ± 74.61 ms (Supplementary Fig. 3g, h), consistent with previous reports [29,31]. We found that firing rates and variations of ISI of LH_{GABA} cells did not differ between NREM sleep and wakefulness epochs (6.71 ± 1.17 Hz and 5.78 ± 0.93 Hz, respectively, $P = 0.20$; coefficient of variation, CV: 0.83 ± 0.05 vs. 1.00 ± 0.07; $P = 0.10$, respectively; $N = 22$ cells, 3 mice). However, LH_{GABA} cells showed a transient increase in firing rate during first 3s after NREM sleep-to-Wake transitions (11 out of 13 cells, 3 mice, $P = 0.02$, binomial test, Supplementary Fig. 3e) but not during subsequent waking epochs, suggesting that the increase of LH_{GABA} cell firing is transient and limited to the behavioral transition. In accordance with this finding, we found that optical stimulation during NREM sleep induced a rapid (< 3 s) transition to wakefulness in ChETA compared to control mice (Fig. 1i), as revealed by the rapid change in cortical activity and muscle tone (Fig. 1g for experimental timeline and representative traces). Latency of behavioral transitions was highly dependent on the frequency of stimulation, 20 Hz and 1 s continuous illumination inducing the fastest transitions (20 Hz YFP 66.38 ± 6.3 s, N = 11; ChETA 2.94 ± 0.4 s, N = 9, t = 8.91 df = 18, $P = 0.0001$; 1s YFP 61.0 ±4.4 s, N= 4, ChETA 3.6 ± 0.30 s, N= 3, t= 11 df= 5, $P = 0.0001$; Fig. 1i). Interestingly, the behavioral response was selective for NREM sleep state, since activation of LH_{GABA} neurons during REM sleep had no effect (Fig. (20 Hz YFP 61.3± 3.9 s N= 8; ChETA 67.7 ± 4.5 s N= 8, t= 1.06 df= 14, $P = 0.3093$; 1s YFP 69.0 ±5.02 s N= 3, ChETA 71.4 ±12.8 s N = 3, t= 0.213 df= 6, $P = 0.8384$, unpaired two-tailed Student's *t*-test; Fig. 1i). Remarkably, sustained activation of LH_{GABA} cells using a semi-chronic optical stimulation paradigm (5-ms light pulses delivered at 20 Hz for 10s, every min. over 1h; Supplementary Fig. 4a, b) of LH_{GABA} neurons systematically increased the number of arousal transition and increased total wakefulness (> 80 % of the total time) in ChETA compared to control animals (ChETA N =8, YFP N= 7, BS N= 7, F (5,28) = 21.48, $P = 0001$, repeated measures followed by Bonfferoni post-hoc test; Supplementary Fig. 4c and BS N = 8, YFP N = 5, ChETA N = 5, F (3,14) = 14.94, $P = 0.0001$, repeated measures ANOVA followed by Bonfferoni post-hoc test; Supplementary Fig. 4d). Furthermore, optogenetic stimulation of a LH_{GABA} cells that express the long-form of the leptin receptor

b (LepRb)[34] produced and opposite sleep behavior (P= 002, unpaired Supplementary Fig. 5a–c). These results showed that optogenetic activation of a subset of LH_{GABA} cells induces rapid arousal from NREM sleep and causes prolonged period of wakefulness.

TRN cells receive monosynaptic inputs from LH_{GABA} neurons

In order to determine the downstream circuitries mediating this rapid arousal response, we mapped LH_{GABA} efferents utilising ChR2-assisted circuit mapping after stereotactic delivery of ChETA-EYFP AAV in the LH of Tg(VGAT)::IRES-Cre mice. We found that LH_{GABA} neurons send projections to various hypothalamic nuclei and long-range projections to sleep-relevant brain nuclei, including the TRN, dorso-medial thalamus, locus coeruleus, neocortex and septum (Fig. 2a; Supplementary Fig. 1a). Surprisingly, LH_{GABA} cells project massively to both the anterior and posterior parts of the TRN where synaptic terminals are in close apposition to GAD-67^{+} cells (Fig. 2a). This monosynaptic LH-TRN connection was further confirmed by separate stereotactic injection of fluorescent beads (Fig. 2b) and LT-HSV-EGFP lentivirus (Supplementary Fig. 6a–d) restricted to the TRN area, both of which showed a retrograde labelling of GABA and non-GABA cell bodies in the LH. We then used optogenetics to functionally characterize this LH_{GABA}-TRN circuit. We found that optical activation of ChETA-YFP-expressing LH_{GABA} terminals faithfully evoked postsynaptic currents (IPSCs, 61.7 ± 12 pA peak amplitude; 111.6 ± 5.7 ms decay time, values represent mean ± SEM) in ~ 80 % of TRN cells recorded (Fig. 2c–f). These currents were bicuculline sensitive (−5.16 ± 0.5 pA peak amplitude), suggesting a major role for $GABA_A$ in LH-TRN synaptic transmission. IPSC latencies were typically short (2.6 ± 0.4 ms) consistent with latencies of monosynaptic connection in hypothalamic circuits[27,35], while the absence of paired-pulse facilitation/depression (Peak 1: −61.7 ± 12 pA; Peak 2: −54.53 ± 10.2 pA; N = 5 cells from 5 different mice, $P = 0.187$, Wilcoxon signed rank test; Fig. 2d, f) suggested a strong GABAergic control from LH_{GABA} neurons and the absence of synaptic short-term plastic changes following optogenetic stimulation.

Activation of LH_{GABA}-TRN recapitulates arousal transition

LH_{GABA} include a heterogenic populations of both wake-and REM sleep-active neurons[31]. Thus, we hypothesized that the transient activity of LH_{GABA}-TRN circuit supports a direct hypothalamic control over TRN cells, and indirectly, over thalamocortical network during sleep-to-wake transitions. To test this, transduced animals were chronically implanted with moveable silicon probes and optical fibers directly above TRN for both simultaneous recordings and optogenetic manipulation of LH_{GABA} terminals (Fig. 3a, b and Supplementary Fig. 7a, b; see Methods). Consistent with previous studies[36], cells recorded in the TRN showed a typical narrow spike waveform (half-trough time: < 0.2 ms; N = 70 cells, 3 mice, Supplementary Fig. 7c–f). Optical activation of LH_{GABA} terminals in the TRN area exerted a strong frequency-dependent inhibitory action on TRN cell activity (Fig. 3c, d; N = 70 cells, 3 animals, F(3,3) = 38.2831, $P = 9.42$ 10e-16, one-way ANOVA followed by Bonfferoni post-hoc test). The firing rate of TRN cells progressively decreased with increasing optical stimulation frequency or duration (20 Hz: 57 out of 70 cells, 3 mice, $P = 1.62$ 10e-10, Wilcoxon signed rank test, P; 2-s continuous illumination: 17 out of 17 cells; 1 animal, t(32,32) = 5.89, $P = 0.0000014$, un-paired two-tailed student's t-test); both fast-and slow-firing cells reduced their firing rate upon optical stimulation of LH_{GABA} terminals

(Supplementary Fig. 7f). Further, we found that the majority of TRN cells displayed state-dependent activity (Fig. 3b, e): the variability of their interspike intervals (CV) was lower (*i.e.*, cells fired more regularly) during spontaneous waking than during NREM sleep (46 out of 70 cells, 3 animals, $P = 3{,}523e\text{-}09$, Wilcoxon signed rank test ; Fig. 3e). The CV changed across states independently of changes in firing rate (Pearson correlation, $P = 0.26$). Cells with and without state-dependent changes of CV displayed similar firing rates (NREM sleep: 6.19 ± 0.71Hz and 4,86 ± 1.08 Hz, respectively, $P = 0.17$; Waking: 7.58 ± 0.81 Hz and 5.54 ± 0.92 Hz, respectively; $P = 0.22$) and mean ISI (275.0 ± 44.83 ms vs. 406.99±77.98 ms, respectively; $P = 0.2$). Optical stimulation of LH_{GABA}-TRN_{GABA} projections replicated state-dependent changes of CV in TRN neurons (20 Hz: N = 46 cells, 3 animals, $P = 0.0086$, Wilcoxon signed rank test ; 2-s continuous illumination: N = 10 cells, 1 animal, $P = 0.00195$, Wilcoxon signed rank test; Fig. 3e and Supplementary Fig. 7g). These results strongly support the hypothesis that inhibition of TRN cells controls NREM sleep-to-wake transitions.

To test whether inhibition of TRN cells affect NREM sleep-to-wake transitions, we quantified the latency of arousal transitions from NREM and REM sleep following optogenetic activation of LH_{GABA} terminals in the TRN in ChETA-YFP and control animals (See Methods). Optical stimuli were delivered at the onset of NREM or REM sleep episodes, as detected by real-time EEG/EMG analysis in freely-moving mice (See Fig. 1g for experimental timeline)[26,27]. We found that bilateral optogenetic stimulation of LH_{GABA} terminals in the anterior part of the TRN during NREM sleep induced a rapid (< 2 s) transition to wakefulness in ChETA compared to control mice (Fig. 3f). The speed of this transition was directly dependent to the frequency of stimulation and the number of light pulses, while brief continuous illumination significantly induced the shortest latency of wake onset (ChETA 2.77 ± 0.299 s, N = 7, *vs* CTRL 63.7 ± 3.84 s, N = 5 t=19.1 df = 10, $P=$ 0.0001, unpaired two-tailed Student's *t*-test; Fig. 3f). Optically induced wakefulness was transient and equal in duration to circadian-matched awake episodes in control animals (on condition: ChETA 18.1 ± 3.92 s, N = 7, *vs* CTRL 15.5 ± 31.70 s, N=5t=0.56 df =11, $P=$ 0.58, unpaired two-tailed Student's *t*-Test; Fig. 3g). Note that stimulation of the posterior part of the TRN showed slightly longer latencies, presumably due to a smaller number of terminals reached by the optical beam (Supplementary Fig. 8a–c). Importantly, we did not observe any behavioral changes with optogenetic stimulation of LH_{GABA}-TRN circuit during REM sleep states (on condition: ChETA 62.1 ± 3.93 s, N = 7, *vs* CTRL 78.1 ± 4.47 s, N= 5 t= 1.96 df =10, $P = 0.078$, unpaired two-tailed Student's *t*-Test; Fig. 3h). State-dependent optogenetic activation of the LH_{GABA}-TRN circuit precisely reproduced behavioral changes observed following activation of LH_{GABA} cells bodies (compare Fig. 1h and Fig. 3f), suggesting that the TRN nuclei is the primary target of LH_{GABA} cells in arousal control during NREM sleep.

In addition and consistent with the widespread projections of LH_{GABA} cells in the locus coeruleus (LC), medial septum (MS) and dorsal thalamus (PVf; Fig. 4a and Supplementary Fig. 1a, b, d), we found that optogenetic stimulation of LH_{GABA} terminals in the MS had no effect on arousal from NREM sleep, whilst their activation in the LC induced arousal from both NREM and REM sleep (Fig. 4b, c). In addition, LH_{GABA} terminals in the PVf nuclei induced arousal from NREM, but not REM sleep with significantly lower efficacy than the

TRN (Fig. 4b, c). These latter data suggest the existence of some functional heterogeneity amongst LH_{GABA} arousal cells. They further confirm that TRN, rather than dorsal thalamus or LC, is primarily involved in fast arousal control from NREM sleep.

Silencing of TRN cells causes arousal

Our results indicate a causal link between the transient activation of LH_{GABA}-TRN circuit and NREM sleep-to-Wake transitions, suggesting that a transient inhibition of TRN cells is required for arousal transition as suggested in vivo (see Fig. 3b, gray box). To test this hypothesis, we transduced TRN cells with ArchT-YFP or YFP (control) AAVs and implanted bilateral optical fibers above the anterior TRN for *in vivo* optical silencing of TRN_{GABA} neurons while recording cortical EEG and EMG signals (Fig. 5a, b; see Fig. 5c for experimental timeline). Expression of the transgene was selective to the TRN, but absent from adjacent thalamic nuclei, which do not contain VGAT-expressing neurons (Fig. 5b). In line with our previous results, we found that optical silencing of TRN cells during NREM sleep induced rapid sleep-to-wake transitions in ArchT-YFP compared to control animals (ArchT: 18.74 ± 1.5 s, N = 6 *vs* CTRL: 64.06 ± 6.2 s, N= 5, t= 8.54 df = 8, P= 10.73, unpaired two-tailed Student's *t*-Test; Fig. 5e), but had no effect on behavioral transitions during REM sleep (ArchT: 54.13 ± 5.3 s N= 6 *vs* CTRL: 67.50 ± 5.1 s N=5, t= 1.79 df =9, P = 0.11, unpaired two-tailed Student's *t*-Test; Fig. 5f) or wake duration (ArchT: 15.7 ± 1.71 s N=6 *vs* CTRL: 30.20 ± 12.4 s N = 4, t= 1.45 df= 8, P = 0.184, unpaired two-tailed Student's *t*-Test; Fig. 5g). This result further confirms that a transient silencing of TRN is required for LH_{GABA} cell-mediated arousal from NREM sleep.

Silencing of LH_{GABA}-TRN stabilizes NREM sleep

Does silencing of LH_{GABA} cells, and their projections to TRN in particular, promote NREM sleep? To test this, LH of Tg(VGAT)::IRES-Cre mice were transduced with AAVs and implanted bilateral optical fibers above the anterior TRN for *in vivo* optical silencing while recording cortical EEG and EMG signals (Fig. 6a, b). Optical continuous pulses were started 10 s after the onset of NREM and continued until the next transition (i.e., Wake or REM sleep; Fig. 6b). We found that bilateral optogenetic silencing of LH_{GABA} terminals in the anterior part of the TRN (using continuous optical illumination; Fig. 6b and c) significantly prolonged the duration of NREM sleep episode in ChETA compared to control mice (ArchT: 117.0 ± 12.13 s, N = 4 *vs* CTRL: 59.21 ± 3.14 s N=4 or spontaneous NREM bout duration ± 5.3, N = 4, F (3,12) = 3.49, P = 0.0001, repeated measures followed by Bonfferoni post-hoc test; Fig. 6e). Interestingly, time-frequency analysis showed that optical silencing induced a significant increase of the amplitude of delta oscillations (0.5–4 Hz; ArchT: 0.118 ± 0.006, N = 4 *vs* CTRL: 0.00872 ± 0.005 s, N = 4, t = 4.42, P= 0.0052, unpaired two-tailed Student's *t*-Test;Fig 6g; see Fig. 6c, d for representative traces), a hallmark of sleep homeostasis[37]. No changes were observed in the spindle frequency domain (ArchT: 0.013 ± 0.0017, N =4 *vs* CTRL: 0.0169 ± 0.0017 s N = 4, t = 1.16, P = 0.28, unpaired two-tailed Student's *t*-Test; Fig 6h). Thus, silencing of LH_{GABA} cells facilitates maintenance of NREM sleep and enhances the process of recovery of sleep.

Activation of LH_{GABA}-TRN induces emergence from anesthesia

Interestingly, the changes in thalamocortical oscillations and cellular activity associated with a transition from sleep to wakefulness share some characteristics with those occurring during emergence from anaesthesia[8]. In particular, experimental evidence has linked the thalamus, and the TRN in particular, to various states of consciousness, including anaesthesia[8]. General anaesthetics (barbiturates, propofol, etc.) at clinically relevant concentrations disinhibit TRN neuron activity and cause a concomitant reduction in firing rate in the thalamus [8,38]. Therefore, we hypothesized that the LH_{GABA}-TRN arousal circuit could be a key structure in modulating thalamocortical oscillations during anaesthesia as well as controlling emergence from anaesthesia. To test this, we optogenetically activated the LH_{GABA}-TRN terminals during progressive isoflurane exposure (0–1.2 %; Fig. 7a) while recording EEG activity and loss of righting reflex (LORR), a surrogate for loss of consciousness in humans (see ref.[39]). Animals were optically stimulated once stable burst-suppression mode was recorded from the cortex (Fig. 7b). We found that a single 5-s bilateral optical stimulation caused a significant increase of the total duration of burst activity in the cortex (ChETA: 35.0 ± 3.7 s N=4 *vs* CTRL 12.1 ± 4.3 s N= 4 in a total time of 60 sec 2 min after stimulation, t = 4.08 df = 6, P= 0.0065, unpaired two-tailed Student's *t*-Test; Fig. 7d). This change persisted for ~ 2 minutes before returning to burst suppression mode (Fig. 7e). In some cases (2 out of 4 animals), optical stimulation during bursting led to emergence from anesthesia accompanied by limb movements and a lack LORR. In contrast, optogenetic stimulation delivered during iso-electric activity had no effects (ChETA: 13.7 ± 2.03 s N=4 *vs* CTRL 8.53 ± 1.74 s N= 4 in a total time of 60 sec 2 min after stimulation; t=1.94 df = 6, P= 0.1003, unpaired two-tailed Student's *t*-Test; Fig. 7f), consistent with their inhibition during that phase of the burst-suppression mode [40]. This result further implicates the TRN in regulating LH_{GABA} activation of the thalamocortical system.

Discussion

The implication of TRN neurons in generating spindle oscillations (11–15 Hz) that characterizes early sleep stage[8,24,36,41] and consolidated NREM sleep[25], suggests a possible role of this structure in modulating the transitions between sleep-wake states and their maintenance.

Here, we showed that a subset of LH_{GABA} cells sends monosynaptic connection to TRN cells using both antero-and retrograde tracing experiments. Based on a qualitative analysis of this mapping, we found that LH_{GABA} cells exert a strong $GABA_A$-mediated inhibitory action on TRN cells during spontaneous NREM sleep-to-Wake transitions. To our knowledge, this is the first identification of a functional GABAergic input to the TRN, as previously suggested *in vitro* [20–22], although other inhibitory inputs of intra-or extra-hypothalamic origin may also be involved. The chemical nature of this subset of TRN-projecting LH_{GABA} neurons remains unclear. Our results suggested that these cells do not include LepRb-expressing GABA neurons, since their activation resulted in an opposite effect and promote NREM sleep. Furthermore, in agreement with the literature[32] and our previous work[27], it is unlikely that those co-express melanin-concentrating hormone peptide – the main marker of LH inhibitory cells-or hypocretins/orexins since those two cell

populations send scarce projections and/or fibers of passage to the TRN region [27,42,43]. Consistent with our *in vivo* recordings indicating that the activity of LH cells is strongly modulated across NREM sleep-to-wake transitions[31], we demonstrated that optogenetic activation of the LH_{GABA}-TRN circuit promotes rapid wakefulness and cortical arousal selectively during NREM sleep and anaesthetized states, respectively, as measured by a prominent change in thalamocortical oscillations (i.e., sudden decrease of the amplitude of < 4Hz oscillations and burst-suppression mode, respectively). This latter result emphasized the potency of the LH_{GABA}-TRN circuit to control thalamocortical oscillations during robust and global burst-suppression cortical oscillations associated with anaesthesia[8].

Our *in vivo* experiments revealed important conceptual findings; firstly, wakefulness transitions induced by activation of the LH_{GABA}-TRN circuit were faster than those induced by optogenetic activation of hypothalamic hypocretin/orexin neurons (LH_{hcrt})[26], and similar to electrical stimulations of the LH area[44] or optogenetic activation of norepinephrine neurons from the locus coeruleus (LC_{NE})[45]. Both the number of synapses within these circuits (LH_{GABA}-TRN *vs* LH_{HCRT}-LC_{NE}-thalamus/Neocortex) and their functional nature (feed-forward inhibition *vs* sequential excitation) might be responsible for their temporal difference in controlling arousal. Secondly, the LH_{GABA}-TRN arousal circuit is specific to NREM sleep since its activation during REM sleep did not result in any noticeable behavioral transitions. This is in contrast with optogenetic activation of LH_{hcrt}[26] and LC_{NE}[45] neurons that induced arousal both from NREM and REM sleep. Consistent with the fact that NREM and REM sleep are controlled by different neurocircuits[2,3], these results strongly suggest a high degree of specialization, rather than redundancy, amongst arousal circuits of the mammalian brain. Thirdly, if optical activation of LH_{GABA}-TRN coincides with isoelectric point of the EEG burst-suppression mode-i.e., when TRN cells are hyperpolarized in anesthetized animals-cortical burst-suppression mode remains unchanged whereas cortical arousal systematically followed when optical stimulation was time-locked with a burst phase. This latter result emphasizes the critical temporal organization of LH_{GABA}-TRN synaptic activity for controlling the activity of the thalamocortical projections.

It is well established that the TRN plays a key role in controlling thalamocortical network oscillations, attention and consciousness[36], however, it has not traditionally been considered as a key node in sleep-wake circuitries. Our results showed that the rapid arousal that occurs upon activation of the LH_{GABA}-TRN circuit is associated with a transient silencing of TRN cell activity. Our results further suggest that a virtual hyperpolarization of TRN cells is required for a temporally-coordinated arousal during NREM sleep (see Fig. 3b, *gray box*). This is indirectly confirmed by the fact that silencing of LH_{GABA}-TRN promotes the maintenance of NREM sleep and enhances the amplitude of delta oscillations, a correlate of sleep intensity and sleep recovery[37,46]. This network effect could result from a dis-inhibition of TRN cells and an enhanced synchronization of thalamocortical and cortical networks.

Collectively, our results identified the LH_{GABA}-TRN_{GABA}-thalamocortical circuit as a novel feed-forward inhibitory circuit that initiates rapid arousal during NREM sleep. During NREM sleep-to-wake transitions, increased activity of LH_{GABA} cells exerts a strong inhibition onto TRN cells, which progressively result in a dis-inhibition of thalamocortical (TC) cells and a switch of TC cell membrane potential from a hyperpolarized (“Down”) to a

more depolarized ("Up") state[1,46–48]. This slow depolarization of TC is associated with the presence of cholinergic, serotonin, norepinephrine and histamine inputs from the brainstem and hypothalamus, respectively, which in parallel also inhibit TRN cells[47]. Thus, it is likely that subcortical inputs are integrated to LH_{GABA} cell signals within the TRN which further controls the activity of thalamic centers, including the intralaminar thalamic (IL) nuclei [49]. Interestingly, we found that direct activation of LH_{GABA}-IL projections resulted in a slower arousal, suggesting a modulatory, rather than a switch function. Specialization amongst thalamic circuitries controlling sensory integration, attention, arousal or wakefulness awaits further investigation.

Our results suggest that the discharge of LH_{GABA} cells is relatively transient at the transition between NREM sleep and wakefulness, suggesting the existence of inhibitory inputs to LH_{GABA} cells. One candidate circuit is a subset of TRN cells that project directly back to the LH area where they exert a rapid (< 2 ms) and strong top-down inhibitory action on a large population (~ 66 %) of LH cell[50]. Alternatively, TC glutamatergic inputs to TRN cells will indirectly provide a negative feedback to TC cells[1,7,11]. These negative feedback loops would repress the firing of LH_{GABA}, or TC, cells, respectively, and avoid uncontrolled hyperactivation of the thalamo-cortical network, and possible pathological states (e.g., epilepsy)[7]. Implication of local and extra-hypothalamic sleep-wake transmitters inputs to LH_{GABA} cells projecting to TRN awaits further investigations. In turn, reactivation of LH_{GABA} cells can occur through local glutamatergic neurons (e.g., hypocretins/orexins cells), as well as extra-hypothalamic arousal circuits from the brainstem. Further functional investigation of the LH-TRN pathway during wakefulness is required to fully elucidate its importance in regulating attention and consciousness.

Online Methods

Animals

Mice used for all expreriments (***Heterozygous Tg(VGAT-Cre) mice were maintained on a 129/SvJ X C57BL/6 genetic background)*** were housed in individual custom-designed polycarbonate cages at constant temperature (22 ± 1 °C), humidity (30–50%), and circadian cycle (12 h light-dark cycle, starting at 8 AM). Food and water were available *ad libitum*. Animals were treated according to protocols and guidelines approved by McGill University and the Canadian Council of Animal Care; Veterinary office of the Canton of Bern, Switzerland; and the Landesamt für Gesundheit und Soziales (LaGeSo, Berlin). Only male mice were used in the behavioral experiments. Mice were housed in groups of 2–4 animals per cage before experiments and after virus injections. After implantations all mice were housed individually. Animals were habituated to the EEG/Optical stimulations in their home cages (30 × 20 cm) and kept plugged for the duration of the experiments. Animals were kept in a rectangular box, 50 × 30 cm and were allowed the mice to freely explore an enclosure during in vivo electrophysiology experiments.

Plasmid and viral targeting

6-weeks old Tg(VGAT)::IRES-Cre male or female mice were anesthetized with isoflurane (5% induction, 1.2–1.5% maintenance) and then placed on a small animal digital stereotaxic

frame (David Kopf Instruments). Only male mice were used for behavioral experiments whereas both male and female mice were used for anatomical and *in vitro* electrophysiological experiments. Mice were randomly assigned to viral injection. 0.6 µl of recombinant AAVdj carrying Ef1α-DIO-ChETA-EYFP or 0.5 µl control Ef1α-DIO-EYFP vector (plasmids were kindly provided by Dr K. Deisseroth, Virus vectors were packaged at Vollum Vector Core, University of Washington) were bilaterally injected in the lateral hypothalamus through an internal 28G cannula (Plastics One) connected to a microinfusion pump (Harvard Apparatus, model 1200) at a rate of 50 nl/min, as previously described[51–53]. Inhibition of TRN cells was done by virally targeting the TRN (anteroposterior (AP), −0.85 mm; mediolateral (ML), ± 1.7 mm; dorsoventral (DV) 3.5 mm) using injections of 0.5 µl of either Ef1α-DIO-ArchT-EYFP Ef1α-DIO-EYFP (controls). Inibition of LH_{GABA} terminals in the TRN was done by injecting Ef1α-DIO-ArchT-EYFP or Ef1α-DIO-EYFP (controls) AAV in the LH (AP), −1.4 mm; mediolateral (ML), ± 1 mm; dorsoventral (DV) 5.4 mm). These Virus vectors were packaged and titered by the University of North Carolina Vector Core Facility.

Slice preparation

P14 Tg(VGAT)::IRES-Cre mice were injected bilaterally using 0.5 µl of Ef1α-DIO-ChETA-EYFP AAV in LH stereotactic coordinates adapted to young animals (AP: −1.40, ML: +/−0.90, DV: 5.35). After completion of the virus injection, mice were retuned to their home cage with the mother for 15–20 days. All mice were anaesthetized using isofluorane inhalation. Brains were collected following decapitation and immediately submerged in an ice cold solution containing (in mM): NaCl 87, KCL 2.5, $NaHCO_3$ 25, $CalCl_2$ 0.5, $MgCl_2$ 7, NaH_2PO_4 1.25, glucose 25, sucrose 75, saturated with 95% O_2/5% CO_2. Brains were blocked and mounted in a vibrating slicer (Leica VT1000S) and kept submerged, ice-cold and oxygenated. Coronal slices from the hypothalamus containing the LH were cut at 300 µM and incubated for 30 minutes at 35°C in artificial cerebrospinal fluid (aCSF) containing (in mM) NaCl 126, KCL 2.5, $NaHCO_3$ 26, $CaCl_2$ 2, $MgCl_2$ 2, NaH_2PO_4 1.25, glucose 10, saturated with 95% O_2/5%CO_2. Then slices were maintained at room temperature with continuous oxygenation. All animals were sacrificed during the light phase and the slices were used during the afternoon at the same circadian time recordings for *in vivo* polysomatic experiments took place.

Individual brain slices were transferred to the recording chamber, and perfused continuously with oxygenated ACSF (1.5–2 ml/min) maintained at 33–35°C using a regulated temperature controller (Model TC324B, Warner Instruments). YFP-expressing neurons in the LH were detected using green light excitation and visualized with an upright microscope (BX51WI, Olympus) equipped with a 40x water-immersion objective, differential interference contrast optics, and a near-infrared fluorescence camera (EXi Blue, Q imaging), and the cells were then identified under IR-DIC. For studies investigating the postsynaptic targets of LH-GABA neurons, slices containing the TRN were observed under both green light excitation and IR-DIC at both 4x and 40x to visualize YFP-positive fibers, only TRN cells in close proximity to fluorescent fibers were selected for recordings. TRN cells were identified based on the electrophysiological fingerprints and anatomical location.

Electrophysiological recordings and data analysis

Both current clamp and voltage clamp configurations were used to describe the electrophysiological characteristics in response to activation of photocurrents in both, GABAergic LH cells, and postsynaptic currents of TRN cells in response to activation of LH-GABA fibres. Whole-cell configuration was done using micropipettes prepared from borosilicate glass capillaries (1.0 mm OD, 0.58 mm ID) using a horizontal puller (P-97, Sutter Instruments), with resistances between 3–5 MΩ. Somatic whole-cell current and voltage clamp recordings from VGAT::CRE neurons were obtained using patch recording pipettes containing (in mM): 120 K-gluconate, 20 KCl, 10 N-2-hydroxyethylpiperazine-N′-2-ethanesulfonic acid (HEPES), 7 phosphocreatine di-Tris, 2 MgCl2, 0.2 ethylene glyco-bis (β-aminoethyl ether)-N,N,N′,N′-tetraacetic acid (EGTA), 4 Na2+-ATP, 0.3 GTP-Tris (pH adjusted to 7.20–7.26 using KOH; 275–285 mOsm). For postsynaptic experiments TRN cells were patched using pipette solution containing (in mM): 108 mM potassium gluconate, 2 mM $MgCl_2$, 8 mM sodium gluconate, 8 mM KCl, 2.5 mM K_2-EGTA, 4 mM K_2-ATP and 0.3 mM Na_3-GTP buffered with 10 mM HEPES. Access resistance was monitored every 2 minutes and cells in which changes were greater than 15% of the initial value (8–10 MΩ) were discarded. TRN cells were voltage-clamped at a holding potential of −70 mV and in the presence of the AMPAR antagonist, CNQX (20 μM). Quantification of the efficacy of somatic responses was don by calculating the total number of action potentials over 10X consecutive stimulation at different frequencies in cells which resting membrane potential was above −58mV. We kept all cells at a holding potential of −60mV thought out the experiment.

For the postsynaptic currents, we use a pair-pulse stimulation paradigm with 50 ms at a rate of 0.2 HZ. We recorded evoked potentials at 50% of the maximum response. For the pharmacological manipulations to assess the action of GABA release from presynaptic LH-GABA terminals on TRN cells, we recorded baseline of 5–10 min before perfusing with bicuculline methiodide (BIC, 10 μM) to block $GABA_A$ receptors 10mM of $GABA_A$ blocker bicuculline. Cells were recorder for 10 min in the presence of the clocker and then washed out. All salts and powders were purchased from Sigma-Aldrich, except for 6-cyano-7-nitroquinoxaline-2,3-dione (CNQX), DL-(±)-2-amino-5-phosphonopentanoic acid (AP-5), and BIC (10 μM) (Ascent Scientific, Princeton, NJ, USA). *In vitro* electrophysiological data were discarded if intrinsic cell properties (resting membrane potential, input resitance) were more than 3SDs outside group mean, and / or if recording stability changed by >15%, as monitored by series resistance measurments throughout the course of the experiment (mean series resistance was 17 ± 1 MΩ).

Surgical procedures for sleep experiments

As described previously[51,53,54], 8–10-weeks male Tg(VGAT)::IRES-Cre mice were chronically implanted with bilateral 200 μm fiber implants above the lateral hypothalamus (MFC_200/245-0.37_5_TF2-FLT; Doric Lenses; AP, 1.45; ML, 0.95 mm; DV, 4.8 mm) and affixed to the skull with C&B Metabond (Patterson dental). Then, a custom-made-EEG/EMG implant was placed posterior to the implant and secured to the skull with dental cement (Patterson dental). EEG signals were recorded from 4 electrodes on the frontal (AP, −2 mm; ML, ± 2.5 mm) and temporal (AP, 3.5 mm; ML, ± 3 mm) cortices. EMG signals

were recorded from two electrodes inserted in the neck musculature to record postural tone. After surgical procedures, mice were allowed to recover in an individual housing cage for at least 2 weeks. After 1 additional week of acclimation to the EEG-EMG recording set up, an optical patch cord (MFP_200/230/900-0.37_2m_FC-ZF1,25) and a zirconia sleeve (ID=1.25; Doric Lenses) were connected permanently on the fiber implant[55]. Black nail polish was applied on the plug to blackout the light during the optogenetic stimulation. The same methods of implantation and habituation were used for animals transduced with ArchT-EYFP in the TRN and LH, and implanted with optical fibers in the TRN.

For the stimulation of the LH_{GABA} targets, a bilateral fiber implant was implanted above the TRN at two different locations (reticular thalamic nucleus; Anterior: AP, −0.85mm, ML, 1.70 mm and DV, −3.4mm; $N = 6$ ChETA and $N = 6$ control; Posterior AP, −1.34 mm, ML, ±2.0 mm and DV, −3.2mm; $N = 7$ ChETA and $N = 6$ control). A single optical fiber with a 6.5° angle was implanted near the medial septum (AP, 0.86 mm, ML, 0.60 mm and DV, −3.62mm; $N = 4$ ChETA and $N = 4$ controls). A single optical fiber was implanted above the PVf (paraventricular thalamic nucleus, AP, −0.86 mm, ML, 0.60 mm and DV, −3.55 mm; $N = 4$ ChETA and $N = 4$ controls). A bilateral optical fiber was implanted above the LC (Locus ceroeulus AP, −5.45 mm, ML, ± 1.0 mm and DV, −3.55 mm; $N = 4$ ChETA and $N = 4$ controls). Position of optical fibers was verified for each animals included in this study. For inhibition of the TRN, fibers where implanted bilaterally at the level of the anterior TRN (Anterior: AP, −0.85mm, ML, 1.70 mm and DV, −3.4mm; $N = 4$ in each group). Inhibition of LH_{GABA} projections in the anterior TRN was done by chronic implantation of bilateral fibres above the anterior TRN (AP, −0.85mm, ML, 1.70 mm and DV, −3.4mm; $N = 4$ in each group). Only animals where fibres and injection sites were accurate were included for data analysis.

For the silicon probe preparations, animals were implanted with single optical fiber fabricated from 100 μm diameter fiber (0.22 NA, Thorlabs, Newton, NJ, USA) in the TRN (angular implantation, AP −0.8, ML, 1.7, DV, 3.4 mm, $N = 3$). For optical stimulation of LH cell bodies, a single optical fiber was implanted in the LH (angular implantation, AP −1.5, ML 1, DV 5 mm, $N = 5$).

Implantations of silicon probes

Octrode probes (B32, NeuroNexus Technologies), mounted on a custom-made microdrive, were used. These were implanted as described in[56,57], above TRN (AP −1, ML 1.2, DV 3.9 mm), gradually advanced to maximize yield of recorded units, and then moved to LH (DV 5 mm). Reference and ground electrodes were miniature stainless-steel screws in the skull above the cerebellum. The implants were secured on the skull with dental acrylic. Electrodes were connected to operational amplifiers (Brain Technology Team, Pecs, Hungary, or Neuralynx) to eliminate cable movement artefacts. Electrophysiological signals were differentially amplified, band-pass filtered (1 Hz–10 kHz, Digital Lynx, Neuralynx) and acquired continuously at 32 kHz. Timestamps of laser pulses were recorded together with electrophysiological signals. After completion of the experiments, mice were deeply anesthetized and electrolytic lesions at selected channels were performed. Brains were kept for histological analysis.

Signal processing and data analysis

Electrophysiological signals were processed using Neurophysiological Data Manager (NDManager[58], http://neurosuite.sourceforge.net/). LFP was obtained by low-pass filtering and down-sampling of the wide-band signal to 1250 Hz. Further data processing was performed by custom-written MATLAB (Mathworks, Natick, MA, USA) algorithms as described elsewhere[56,57].

Laser pulse timestamps and borders of stimulation epochs were detected. Action potentials were detected in a band-pass filtered signal (0.8 kHz–5 kHz). Events with a magnitude exceeding 3 SD above mean were detected; spike waveforms were extracted and represented by the first 3 principle components. Spike sorting was performed automatically followed by manual clusters adjustment[59]. Putative LH GABAergic interneurons were identified based on rapid (<10 ms in laser pulse onset-triggered cross-correlations) significant increase of firing rate upon laser pulse onset compared to a pre-pulsebaseline. TRN neurons had typical narrow spike waveform (half-trough time<0.2 ms)[60]. Single-(with a refractory period >= 2 ms) and multi-units, recorded in TRN and LH, were used in further analysis.

Polysomnographic recordings and state transitions

All sleep experimental procedure took place between 12:00 and 19:00 (light onset at 8:00). EEG and EMG signals derived from the surgically implanted electrodes were amplified (Grass Instruments) and digitized at 512 Hz using sleep recording software (Vital Recorder, Kissei Comtec). The signals were digitally filtered and spectrally analyzed by fast Fourier transformation. Polysomnographic recordings were scored using sleep analysis software (SleepSign for Animal, Kissei Comtec). All scoring was performed manually based on the visual signature of the EEG and EMG waveforms, as well as the power spectra of 5-s epochs, as previously described[51,54,61]. We defined wakefulness as desynchronized low-amplitude EEG and high tonic EMG activity with phasic bursts. We defined NREM sleep as synchronized, high-amplitude, low-frequency (0.5–4 Hz) EEG and highly reduced EMG activity compared with wakefulness with no phasic bursts. We defined REM sleep as having a pronounced theta rhythm (6–9 Hz) and a flat EMG. State transitions were identified when EEG/EMG criterion change were predominant for more than 50% of the epoch duration (i.e., 2 s). As previously described[12], polysomnographic scorings were tested by two independent scorers and was found to lie within a 95% confidence interval.

In vivo optogenetic stimulations of LH and TRN areas were conducted during NREM or REM sleep using real-time EEG/EMG detection after 10 seconds of the onset of NREM sleep and 5 s of REM sleep and described in[62]. Note that animals with aberrant circadian distribution of sleep-wake cycle (< 10 %) were discarded from this study and that genetic and viral manipulations did not disrupt spontaneous sleep-wake architecture compared to naïve and wild type animals.

For sleep recordings performed in combination with the in vivo electrophysiology, sleep scoring was performed in Spike 5, using the Sleepscore v1.01 script.

The statistical significance of comparisons was determined by T-test (α adjusted for multiple comparisons) or Kruskal Wallis test; P-values<0.05 were considered to indicate significance.

Optogenetic stimulation

For *in vitro* electrophysiology stimulation, somatic and postsynaptic currents were evoked by delivering 5-ms square pulses of blue light (473 nm) delivered to the acute brain slice. We use a diode-pumped solid-state lasers (DPSSL, Laserglow, Toronto, ON) connected to a 200 μm optical fiber (ThorLabs) aimed at the target region. Pulse durations and frequencies were triggered via a built-in TTL circuit controlled by Clampex 10.3 software package. Light intensity was tested before each experiment, and was calibrated to emit 5 mW from the fibre tip.

For *in vivo* optogenetic stimulation electrophysiological experiments, a 3-m long fiber optic patch cord with protective tubing (Thorlabs) was connected to a chronically implanted optical fiber with a zirconia sleeve (Precision Fiber Products, Milpitas, CA, USA)) during optical stimulation. The patch cord was connected to a 473 nm DPSS laser (R471005FX, Laserglow Technologies, Toronto, ON, Canada) with an FC/PC adapter. The laser output was controlled using a stimulus generator and MC_Stimulus software (Multichannel Systems, Reutlingen, Germany). Optical stimulation of LH_{GABA}-TRN projections consisted of blue (473 nm) light pulses at a light power output of 25–30 mW from the tip of the patch cord measured with a power meter (PM100D, Thorlabs). For the characterization of TRN cells response to stimulation of LH GABA-TRN projections, blue light was delivered at 1, 5 or 20 Hz for 40 seconds each, or in 2-s pulses during 2 minutes. For the characterization of LH cells response to stimulation of LH_{GABA} cell bodies, blue light of 5 ms pulses for 10 s at various frequencies was delivered with light power output of 25–30 mW from tips of the optic fibers, as mice freely explored an enclosure.

Optical stimulation during polysomnographic recordings

Animals were kept tethered with the EEG recording cable and the fiber optic patch cord with protective tubing as descried above. During the stimulation session, animals were left to sleep and during sleep periods, light was delivered at 5-ms square pulses at 1, 20 Hz or 1-s continuous light (473 blue laser) using a Master 9 pulse generator (A.M.P Instruments, LTD) (ChETA experiments) or continuously for 5 seconds in the case of the inhibition of the TRN (593 nm yellow laser) and anaesthesia experiments (light activation of LH_{GABA} terminals with 473 blue laser). Similarly to the inhibition of the LH_{GABA} terminals in the TRN experiment, was done by delivering light continuously throughout the duration of NREM sleep. During the experiment, frequencies of optogenetic stimulations (1 and 20 Hz) were randomly delivered at either NREM or REM sleep onset in Tg(VGAT)::IRES-Cre and control mice. Animals with no viral expression, abnormal sleep-wake cycle (3SD outside group mean) or optical fiber/probe implants outside the target area were discarded from the study. Based on these criteria, 4 ChETA, 3 EYFP, 1 ArchT transduced Tg(VGAT)::IRES-Cre animals were excluded from the study. Data collection and analysis were not performed blind to the conditions of the experiments.

Spectral EEG/EMG analysis

For all EYF and ArchT-EYFP transduced mice used for state-specific stimulations, EEG power spectra were computed for 6 to 10 stimulated events per animal (more than 20 s duration). EEG activity recorded during these events was digitized and subjected to the fast

Fourier transform (512 points) using SleepSign software. Mean spectral density of all the stimulated events per animal was sorted into successive 0.062 Hz frequency bands between 0 and 100 Hz, then each frequency band was normalized to the sum of the power over the entire range (0–100 Hz). Frequency EEG bands are defined as delta (0.5–4 Hz), theta (6–9 Hz), alpha (9–12 Hz), spindle (11–15Hz), sigma (12–20 Hz), low gamma (20–60 Hz) and fast gamma (60–100 Hz). Time-frequency power spectrums (inhibition of LH_{GABA} projections in the anterior TRN and anaesthesia experiment) were copmuted using Matlab and the Chronux signal processing toolbox[63].

Anaesthesia experiments

Male mice transduced with YFP and ChETA viral vectors ($N = 4$ in each group) and used in sleep recording experiments were anaesthetised using a induction chamber equipped with gas sampling analyzer (DATEX) to monitored the isoflurane delivered and keeping stable levels of anaesthetic throughout the experiments. We recorded 5 min of baseline when the mice were awake. Following that, we induced the mice to an anaesthetized state (lost of righting reflex and in the EEG recording characterized by a burst suppression mode) at a level of isoflurane 1–1.2%; and recorded for 10 minutes of stable anaesthesia (concentration of isoflurane and burst suppression ratio were constant and stable, respectively). Animals were optically stimulated with a single pulse of 5 s continuous illumination in triplicate session. We quantify the total length of each burst (Fig. 7d). Burst suppression ration was calculated by taking the total burst duration time divided by the total time of isoelectric EEG signal. Values were computed taking epochs of 2 minutes before and 4 minutes after the stimulation. We compared the response between animals transduced with ChETA and YFP viruses. Burst length was calculated using Spike 2 (Cambridge electronic design limited data acquisition and analysis software). A burst was detected if it has value superior to 2X S.D. value of the mean amplitude of isoelectric EEG signal. Power spectrum was done using a custom-made Matlab script.

Immunohistochemistry

After completion of experiments, mice were deeply anesthetized with ketamine/xylazine/acepromazide (100, 16 and 3 mg per kg, respectively, intraperitoneal injection) and perfused transcardially with 1× PBS-heparine 0.1%, pH 7.4, followed by 4% paraformaldehyde in PBS. The brains were extracted, postfixed overnight in the same fixative at 4 °C, and cryoprotected in 30% sucrose dissolved in PBS for an additional 24 h at 4 °C. Each brain was sectioned at 40 μm using a cryostat (Leica Microsystems) and collected in PBS with 0.1% Triton X-100 (PBST).

For double immunolabeling, brain sections from virally-transduced mice were washed in PBST for 10 min at room temperature. Sections were then incubated in a blocking solution composed of PBST with 4% bovine serum albumin for 1 h at room temperature. Sections were first incubated for 48 hr at 4 °C in a rabbit anti-YFP (1:5000, Ab290, Abcam) in blocking solution. For figures 2a and 5a, b, co-labelling with mouse anti-GAD67 (1:2000, MAB546, Millipore, Lot # 2350525) was used followed by 5 × 10 min in 1× in PBST, sections were incubated in a solution of Alexa 488 Donkey anti-rabbit IgG secondary antibody (1:1000, A21206, Invitrogen) and Alexa 555 goat anti-mouse IgG secondary

antibody and in PBST for 1 h at room temperature. Sections were washed 3 × 10min in 1× PBST, mounted onto glass slides, and coverslipped with Fluoromount-G (0100-01, Southern Biotech.). Quantification of colocalization was performed on adjacent sections containing LH and throughout the brain in a total of $N = 13$ brains included in Supplementary Fig. 1b–d Brains from silicon probe recordings were were fixed overnight in 4% PFA, equilibrated in 1% PBS for an additional night and finally cut in 50 μm slices using an oscillating tissue slicer (EMS 4500, Electron Microscopy Science, Hatfield, PA, USA). Brain slices were mounted (Flouromount Aqueous Mounting Medium, Sigma-Aldrich, St Louis, MO, USA).

Fluorescence in situ hybridization

Virally transduced brains from 8-weeks male or female mice ($N = 4$) were flash frozen. Brains were cut in coronal sections (16 μm) and mounted onto glass slides for further hybridization with GAD-67 antisense probe followed by immunodetection of YFP fluorescent protein (antibody described above), as described[62]. Co-localization was quantified by counting the total number of cells in the field of view using a 40X objective that were GAD-67+/YFP +. Experiment was repeated 5 times. Brain sections that had no fluorescent expression in the LH area (one mice) were discarded for the quantification shown in Supplementary Fig 1c.

Retrograde labeling

Male or female Tg (VGAT)::IRES cre mice were injected with 0.5 μl of AAVdj Ef1α-DIO-EYFP at 6 weeks of age. 2 weeks later red fluorescence retrograde beads (Lumaflour Inc) were injected in the anterior part of the TRN (AP, −0.85mm; ML, 1.70 mm; DV, −3.4mm). After an additional 2 weeks of incubation, brains were collected as describe above for immunohistochemical labeling. A separate set of mice were injected with AAV2 Ef1α-DIO-mCherry at 6 weeks and with LT-HSV-EGFP lentivirus at 8 weeks. Brains were collected, perfused and processed for immunohistochemistry (see above) two weeks after the last lentiviral injection.

Microscopy

Non-confocal images were collected on a Axio Observer Carl Zeiss fluorescent microscope using fluorescent reflected light except for images in Supplementary Fig S4a and S7a were taken on an Olympus BX 61 microscope (2X/0.06 NA 10X/0.3 NA, 20X/0.5 NA, dry). Confocal images were collected on a LSM 710 Carl Zeiss confocal microscope. Digital images were minimally processed using Image J or Zen to enhance brightness and contrast for optimal representation of the data. All digital images were processed in the same way between experimental conditions to avoid artificial manipulation between different datasets.

Statistical analysis

Statistical analyses of electrophysiological properties and synaptic responses were assessed using repeated measures ANOVAs, paired t-tests, and significant effects were investigated using pairwise multiple comparisons using Student-Newman-Keuls method for parametric data, unless otherwise indicated. Data are presented as mean ± SEM. The statistical significance of comparisons for sleep/silicon multiunit recordings was determined by T-test

(α adjusted for multiple comparisons) or Kruskal Wallis test; P-values<0.05 were considered to indicate significance. All data were analyzed using Prism 5.0 (GraphPad Software), Clampfit 10.3 (Axon Instruments) unless otherwise mentioned. Data were exported into Adobe Illustrator CS3 (Adobe Systems) for preparation of figures. Data distribution was assumed to be normal but this was not formally tested. Experimental sample size were defined based on previous studies [51,62,64]. No statistical methods were used to pre-determine sample sizes.

A supplementary methods checklist is available.

Supplementary Material

Refer to Web version on PubMed Central for supplementary material.

Acknowledgments

We thank the Tidis Lab members for their technical help and comments on a previous version of the manuscript. We thank the laboratory of Prof. H.-R. Widmer for the use of the fluorescence microscope and the animal facility personal at the Douglas Research Center. Optogenetic plasmids were kindly provided by Dr K. Deisseroth. LT-HSV-GFP were kindly provided by Dr M. Mameli. C.G.H. was supported by a Strauss Clinical Fellowship. A. A. and T. K. were supported by the Human Frontier Science Program (RGY0076/2012). A. A. was supported by the Douglas Foundation, McGill University, Canadian Fund for Innovation (CFI), Canadian Research Chair (CRC Tier 2), Canadian Institute for Health Research (CIHR) and the Natural Science and Engineering Council of Canada (NSERC), Inselspital and University of Bern. T.K. and A.P. were supported by the Deutsche Forschungsgemeinschaft (DFG; Exc 257 NeuroCure, T.K. and A.P.; SPP1665, A.P.).

References

1. Steriade M. The corticothalamic system in sleep. Front Biosci. 2003; 8:d878–99. [PubMed: 12700074]
2. Lee SH, Dan Y. Neuromodulation of brain states. Neuron. 2012; 76:209–222. [PubMed: 23040816]
3. Saper CB, Fuller PM, Pedersen NP, Lu J, Scammell TE. Sleep State Switching. Neuron. 2010; 68:1023–1042. [PubMed: 21172606]
4. Steriade M, Nuñez A, Amzica F. A novel slow (< 1 Hz) oscillation of neocortical neurons in vivo: depolarizing and hyperpolarizing components. Journal of Neuroscience. 1993; 13:3252–3265. [PubMed: 8340806]
5. Timofeev I, Chauvette S. Thalamocortical oscillations: local control of EEG slow waves. Curr Top Med Chem. 2011; 11:2457–2471. [PubMed: 21906018]
6. Lőrincz ML, et al. A Distinct Class of Slow (0.2–2 Hz) Intrinsically Bursting Layer 5 Pyramidal Neurons Determines UP/DOWN State Dynamics in the Neocortex. J Neurosci. 2015; 35:5442–5458. [PubMed: 25855163]
7. Huguenard JR, McCormick DA. Thalamic synchrony and dynamic regulation of global forebrain oscillations. Trends in Neurosciences. 2007; 30:350–356. [PubMed: 17544519]
8. Fuentealba P, Steriade M. The reticular nucleus revisited: intrinsic and network properties of a thalamic pacemaker. Progress in Neurobiology. 2005; 75:125–141. [PubMed: 15784303]
9. Cox CL, Huguenard JR, Prince DA. Nucleus reticularis neurons mediate diverse inhibitory effects in thalamus. Proc Natl Acad Sci USA. 1997; 94:8854–8859. [PubMed: 9238067]
10. Kim U, Sanchez-Vives MV, McCormick DA. Functional dynamics of GABAergic inhibition in the thalamus. Science. 1997; 278:130–134. [PubMed: 9311919]
11. Golshani P, Liu XB, Jones EG. Differences in quantal amplitude reflect GluR4-subunit number at corticothalamic synapses on two populations of thalamic neurons. Proc Natl Acad Sci USA. 2001; 98:4172–4177. [PubMed: 11274440]

12. Knyihar-Csillik E, Chadaide Z, Mihaly A, Krisztin-Peva B, Csillik B. Effect of electrical stimulation of the reticular nucleus of the rat thalamus upon c-fos immunoreactivity in the retrosplenial cortex. Ann Anat. 2005; 187:245–249. [PubMed: 16130823]
13. Pita-Almenar JD, Yu D, Lu HC, Beierlein M. Mechanisms underlying desynchronization of cholinergic-evoked thalamic network activity. J Neurosci. 2014; 34:14463–14474. [PubMed: 25339757]
14. Sun YG, et al. Biphasic cholinergic synaptic transmission controls action potential activity in thalamic reticular nucleus neurons. J Neurosci. 2013; 33:2048–2059. [PubMed: 23365242]
15. Cox CL, Huguenard JR, Prince DA. Peptidergic modulation of intrathalamic circuit activity in vitro: actions of cholecystokinin. Journal of Neuroscience. 1997; 17:70–82. [PubMed: 8987737]
16. Brill J, Kwakye G, Huguenard JR. NPY signaling through Y1 receptors modulates thalamic oscillations. Peptides. 2007; 28:250–256. [PubMed: 17196708]
17. Le Masson G, Renaud-Le Masson S, Debay D, Bal T. Feedback inhibition controls spike transfer in hybrid thalamic circuits. Nature. 2002; 417:854–858. [PubMed: 12075353]
18. Hill S, Tononi G. Modeling sleep and wakefulness in the thalamocortical system. J Neurophysiol. 2005; 93:1671–1698. [PubMed: 15537811]
19. Destexhe A, Contreras D, Sejnowski TJ, Steriade M. Modeling the control of reticular thalamic oscillations by neuromodulators. Neuroreport. 1994; 5:2217–2220. [PubMed: 7881030]
20. Browne SH, et al. Kinetic and pharmacological properties of GABA(A) receptors in single thalamic neurons and GABA(A) subunit expression. J Neurophysiol. 2001; 86:2312–2322. [PubMed: 11698521]
21. Huntsman MM, Huguenard JR. Fast IPSCs in rat thalamic reticular nucleus require the GABAA receptor beta1 subunit. J Physiol (Lond). 2006; 572:459–475. [PubMed: 16469775]
22. Schofield CM, Huguenard JR. GABA affinity shapes IPSCs in thalamic nuclei. J Neurosci. 2007; 27:7954–7962. [PubMed: 17652586]
23. Macdonald KD, Fifkova E, Jones MS, Barth DS. Focal stimulation of the thalamic reticular nucleus induces focal gamma waves in cortex. J Neurophysiol. 1998; 79:474–477. [PubMed: 9425216]
24. Halassa MM, et al. Selective optical drive of thalamic reticular nucleus generates thalamic bursts and cortical spindles. Nat Neurosci. 2011; 14:1118–1120. [PubMed: 21785436]
25. Kim A, et al. Optogenetically induced sleep spindle rhythms alter sleep architectures in mice. Proc Natl Acad Sci USA. 2012; 109:20673–20678. [PubMed: 23169668]
26. Adamantidis AR, Zhang F, Aravanis AM, Deisseroth K, de Lecea L. Neural substrates of awakening probed with optogenetic control of hypocretin neurons. Nature. 2007; 450:420–424. [PubMed: 17943086]
27. Jego S, et al. Optogenetic identification of a rapid eye movement sleep modulatory circuit in the hypothalamus. Nat Neurosci. 2013; 16:1637–1643. [PubMed: 24056699]
28. Kempadoo KA, et al. Hypothalamic neurotensin projections promote reward by enhancing glutamate transmission in the VTA. J Neurosci. 2013; 33:7618–7626. [PubMed: 23637156]
29. Nieh EH, et al. Decoding Neural Circuits that Control Compulsive Sucrose Seeking. Cell. 2015; 160:528–541. [PubMed: 25635460]
30. Bonnavion P, Jackson AC, Carter ME, de Lecea L. Antagonistic interplay between hypocretin and leptin in the lateral hypothalamus regulates stress responses. Nat Commun. 2015; 6:6266. [PubMed: 25695914]
31. Hassani OK, Henny P, Lee MG, Jones BE. GABAergic neurons intermingled with orexin and MCH neurons in the lateral hypothalamus discharge maximally during sleep. Eur J Neurosci. 2010; 32:448–457. [PubMed: 20597977]
32. Jennings JH, et al. Visualizing hypothalamic network dynamics for appetitive and consummatory behaviors. Cell. 2015; 160:516–527. [PubMed: 25635459]
33. Vong L, et al. Leptin Action on GABAergic Neurons Prevents Obesity and Reduces Inhibitory Tone to POMC Neurons. Neuron. 2011; 71:142–154. [PubMed: 21745644]

34. Leinninger GM, et al. Leptin acts via leptin receptor-expressing lateral hypothalamic neurons to modulate the mesolimbic dopamine system and suppress feeding. Cell Metabolism. 2009; 10:89–98. [PubMed: 19656487]
35. Schöne C, Apergis-Schoute J, Sakurai T, Adamantidis A, Burdakov D. Coreleased orexin and glutamate evoke nonredundant spike outputs and computations in histamine neurons. Cell Rep. 2014; 7:697–704. [PubMed: 24767990]
36. Halassa MM, et al. State-Dependent Architecture of Thalamic Reticular Subnetworks. Cell. 2014; 158:808–821. [PubMed: 25126786]
37. Borbély AA, Achermann P, Trachsel L, Tobler I. Sleep initiation and initial sleep intensity: interactions of homeostatic and circadian mechanisms. J Biol Rhythms. 1989; 4:149. [PubMed: 2519586]
38. Andrada J, Livingston P, Lee BJ, Antognini J. Propofol and etomidate depress cortical, thalamic, and reticular formation neurons during anesthetic-induced unconsciousness. Anesth Analg. 2012; 114:661–669. [PubMed: 22190559]
39. Zhang Z, et al. Neuronal ensembles sufficient for recovery sleep and the sedative actions of α2 adrenergic agonists. Nat Neurosci. 2015; 18:553–561. [PubMed: 25706476]
40. Steriade M, Contreras D, Curró Dossi R, Nuñez A. The slow (< 1 Hz) oscillation in reticular thalamic and thalamocortical neurons: scenario of sleep rhythm generation in interacting thalamic and neocortical networks. J Neurosci. 1993; 13:3284–3299. [PubMed: 8340808]
41. Contreras D, Curró Dossi R, Steriade M. Electrophysiological properties of cat reticular thalamic neurones in vivo. J Physiol (Lond). 1993; 470:273–294. [PubMed: 8308730]
42. Peyron C, et al. Neurons containing hypocretin (orexin) project to multiple neuronal systems. J Neurosci. 1998; 18:9996–10015. [PubMed: 9822755]
43. Bittencourt JC, et al. The melanin-concentrating hormone system of the rat brain: An immuno-and hybridization histochemical characterization. J Comp Neurol. 1992; 319:218–245. [PubMed: 1522246]
44. Tortorella S, Rodrigo-Angulo ML, Núñez A, Garzón M. Synaptic interactions between perifornical lateral hypothalamic area, locus coeruleus nucleus and the oral pontine reticular nucleus are implicated in the stage succession during sleep-wakefulness cycle. Front Neurosci. 2013; 7:216. [PubMed: 24311996]
45. Carter ME, et al. Tuning arousal with optogenetic modulation of locus coeruleus neurons. Nat Neurosci. 2010; 13:1526–1533. [PubMed: 21037585]
46. Vyazovskiy VV, et al. Cortical firing and sleep homeostasis. Neuron. 2009; 63:865–878. [PubMed: 19778514]
47. McCormick DA, Bal T. Sleep and arousal: thalamocortical mechanisms. Annu Rev Neurosci. 1997; 20:185–215. [PubMed: 9056712]
48. Contreras D, Timofeev I, Steriade M. Mechanisms of long-lasting hyperpolarizations underlying slow sleep oscillations in cat corticothalamic networks. J Physiol (Lond). 1996; 494(Pt 1):251–264. [PubMed: 8814619]
49. Giber K, et al. A subcortical inhibitory signal for behavioral arrest in the thalamus. Nat Neurosci. 2015; 18:562–568. [PubMed: 25706472]
50. Barone FC, Cheng JT, Wayner MJ. Reticular thalamic inhibitory input to lateral hypothalamic neurons: a functional and histochemical determination. Brain Res Bull. 1994; 33:575–582. [PubMed: 8187000]
51. Adamantidis AR, Zhang F, Aravanis AM, Deisseroth K, de Lecea L. Neural substrates of awakening probed with optogenetic control of hypocretin neurons. Nature. 2007; 450:420–424. [PubMed: 17943086]
52. Mechanism for Hypocretin-mediated sleep-to-wake transitions. Proc Natl Acad Sci USA. 2012; 109:E2635–44. [PubMed: 22955882]
53. Sleep homeostasis modulates hypocretin-mediated sleep-to-wake transitions. J Neurosci. 2009; 29:10939–10949. [PubMed: 19726652]
54. Adamantidis A, et al. Sleep architecture of the melanin-concentrating hormone receptor 1-knockout mice. Eur J Neurosci. 2008; 27:1793–1800. [PubMed: 18380672]

55. Construction of implantable optical fibers for long-term optogenetic manipulation of neural circuits. 2012; 7:12–23.

56. Wulff P, et al. Hippocampal theta rhythm and its coupling with gamma oscillations require fast inhibition onto parvalbumin-positive interneurons. Proc Natl Acad Sci USA. 2009; 106:3561–3566. [PubMed: 19204281]

57. Korotkova T, Fuchs EC, Ponomarenko A, Engelhardt von J, Monyer H. NMDA receptor ablation on parvalbumin-positive interneurons impairs hippocampal synchrony, spatial representations, and working memory. Neuron. 2010; 68:557–569. [PubMed: 21040854]

58. Hazan L, Zugaro M, Buzsáki G. Klusters, NeuroScope, NDManager: a free software suite for neurophysiological data processing and visualization. J Neurosci Methods. 2006; 155:207–216. [PubMed: 16580733]

59. Harris KD, Henze DA, Csicsvari J, Hirase H, Buzsáki G. Accuracy of tetrode spike separation as determined by simultaneous intracellular and extracellular measurements. J Neurophysiol. 2000; 84:401–414. [PubMed: 10899214]

60. Halassa MM, et al. State-Dependent Architecture of Thalamic Reticular Subnetworks. Cell. 2014; 158:808–821. [PubMed: 25126786]

61. Franken P, Chollet D, Tafti M. The homeostatic regulation of sleep need is under genetic control. J Neurosci. 2001; 21:2610–2621. [PubMed: 11306614]

62. Jego S, et al. Optogenetic identification of a rapid eye movement sleep modulatory circuit in the hypothalamus. Nat Neurosci. 2013; 16:1637–1643. [PubMed: 24056699]

63. Bokil H, Andrews P, Kulkarni JE, Mehta S, Mitra PP. Chronux: A platform for analyzing neural signals. J Neurosci Methods. 2010; 192:146–151. [PubMed: 20637804]

64. Schöne C, Apergis-Schoute J, Sakurai T, Adamantidis A, Burdakov D. Coreleased orexin and glutamate evoke nonredundant spike outputs and computations in histamine neurons. Cell Rep. 2014; 7:697–704. [PubMed: 24767990]

65. Hassani OK, Henny P, Lee MG, Jones BE. GABAergic neurons intermingled with orexin and MCH neurons in the lateral hypothalamus discharge maximally during sleep. Eur J Neurosci. 2010; 32:448–457. [PubMed: 20597977]

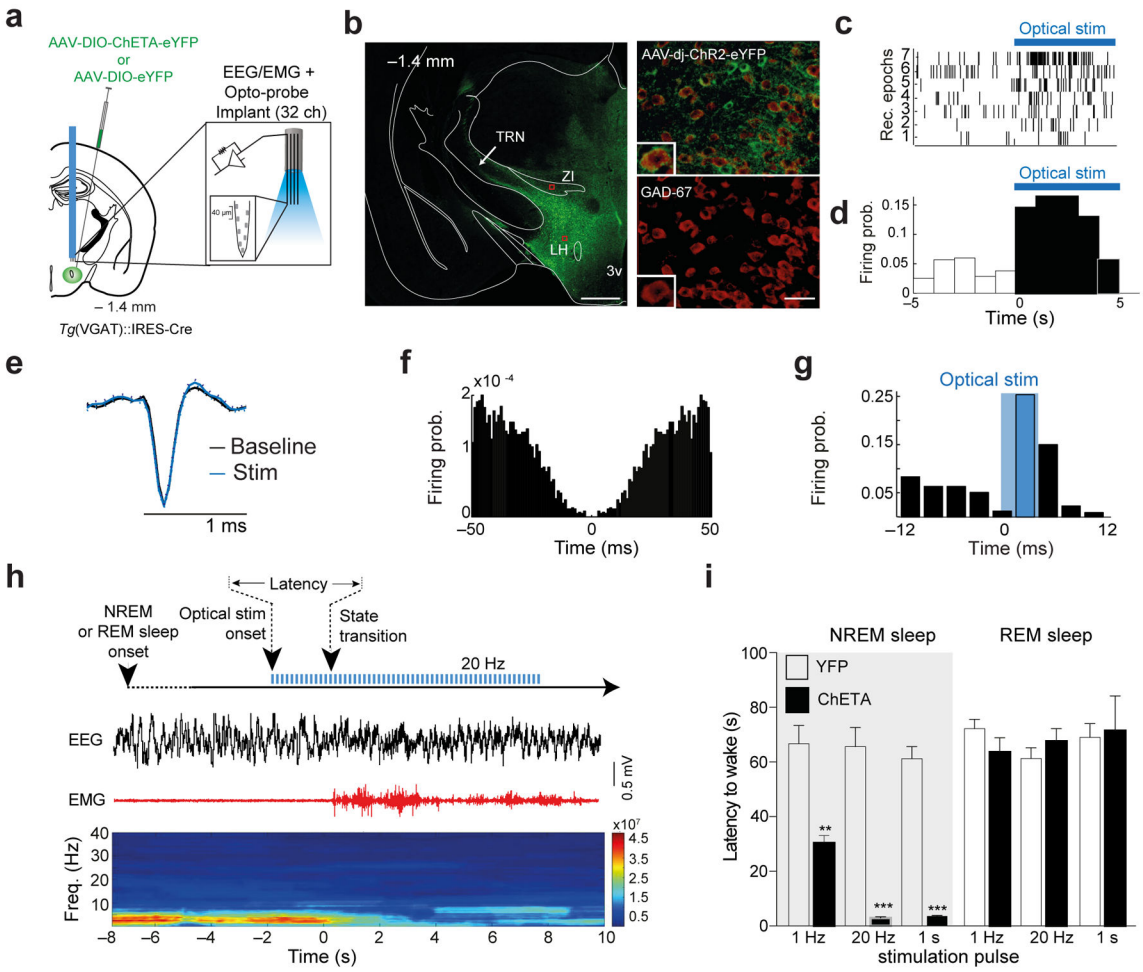

Figure 1. LH_{GABA} neurons control rapid arousal

a, Schematic of the genetic targeting and optoprobe used or stimulation/recording. AAVdj-DIO-ChETA-YFP or AAVdj-DIO-YFP (Control) were infused into the lateral hypothalamus (LH) of tg(VGAT)::IRES cre mice (*left*). **b**, Photomicrograph showing the selective targeting of ChETA-YFP expression in GAD-67+ neurons in the LH (*right panels*). Scale bar: 500 μm (left), 20 μm (right). Representative images from repeated experiment (>15 sections from *N* = 4 transduced mice). **c,** Examples of optostimulation onset-triggered rastergrams of representative 7 LH cells (top; of 31 recorded presumable LH_{GABA} cells) and their firing probability before and after the optostimulation onset (**d**). **e**, Average spike waveforms (top) of a representative presumable ChETA-expressing LH_{GABA} cell before (black) and during optostimulation at 20 Hz (blue). **f,** Auto-correlogram of the unit shown in (**e**). Traces were obtained from 3 different recordings, *N*=2 mice. **g**, Firing probability of a presumable ChETA-expressing LH_{GABA} cell in response to optostimulation. Cross-correlation bin width: 3 ms. **h**, Schematic of the experimental timeline (top). Representative EEG/EMG traces and the corresponding heat map EEG power spectrum illustrate behavioural response to optogenetic stimulation. Note the decrease of the power (color axis, mV^2/Hz) of low frequency (< 4 Hz) oscillations and the EMG tone during the NREM-to-Wake transition. **i,** Mean latencies ± S.E.M of NREM (*left*) (1Hz *N* = 9 ChETA, YFP *N* = 10, t=4.84 df=17, *P*=

0.0002; 20Hz $N = 9$ ChETA, YFP $N = 11$, t=8.91 df=18, $P = 0.00001$, 1 s $N = 3$ ChETA, YFP $N = 4$, t=11 df=5, $P = 0.0001$) and REM (*right*)) (1Hz $N = 8$ ChETA, YFP $N = 10$, t=0.213 df=6, $P = 0.173$; 20Hz $N = 8$ ChETA, YFP $N = 8$, t=4.36 df=4.04, $P = 0.39$, 1 s $N = 3$ ChETA, YFP $N = 5$, t=0.0838 df=8, $P = 0.8384$, Data analysis based on > 15 stimulations per frequency and per animal (N). significance was determined as when P values were **, $P < 0.001$, ***, $P < 0.0001$ using unpaired two-tailed Student's *t*-Test).

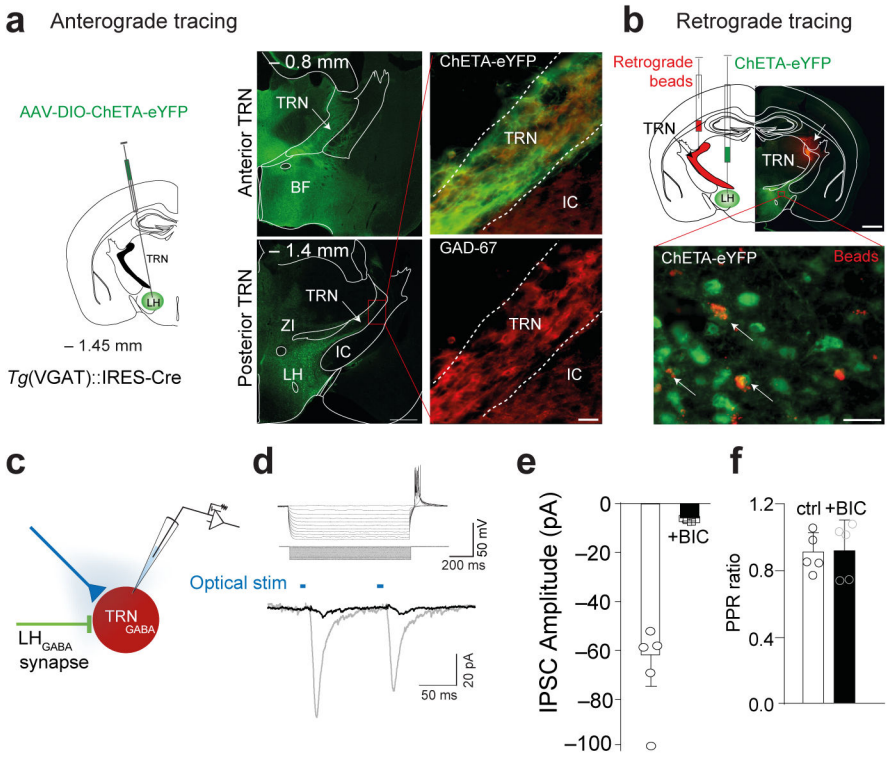

Figure 2. Identification of a monosynaptic LH_{GABA}-TRN circuit

a, Anterograde tracing of LH_{GABA} projections to the TRN area. Schematic of a coronal hemisection (left) illustrating the injection of AAV-DIO-ChETA at the level of the LH injection (AP: −1.45 mm). Photomicrograph of coronal section showing anterograde labelling of ChETA-EYFP-expressing LH_{GABA} axons in the anterior and posterior TRN (*middle, top and bottom panels*). Scale bar: 500 μm. Photomicrograph magnification of coronal section showing the overlap of ChETA-EYFP expressing LH_{GABA} terminals intermingled with GAD-67+ cells in the posterior TRN (*right, top and bottom panels)*. Scale bar: 20 μm. Genetic targeting was confirmed in animals included in the behavioural study using immunohistochemistry. **b**, Retrograde tracing of LH_{GABA} projections to the TRN area. Schematic coronal hemisection (top, left) of the experimental approach. Photomicrograph of a coronal hemisection at the level of the LH (AP: −1.45 mm) showing injection site of retrograde beads (red) in the TRN and ChETA-expressinf cells in the LH (right, top). Scale bar: 200 μm. *Bottom*, Photomicrograph magnification of the red box in top panel showing EYFP-expressing LH_{GABA} cell bodies (green) retrogradely labelled with beads (red). White arrows indicate YFP-positive LH_{GABA} cells projecting monosynaptically to the TRN. Representative images from repeated experiment (> 15 sections from $N = 4$ transduced mice). **c**, Optogenetic-assisted circuit mapping of LH_{GABA}-TRN circuit. **d**, Electrophysiological fingerprint of TRN cell (top) in response to a series current steps (*inset*). Whole cell voltage-clamp recordings (bottom) show robust bicuculine (BIC)-sensitive (*red traces*) inward photocurrents (*black traces*) evoked by single 5-ms 473 nm light pulses. **e**, Group data representing mean ± S.E.M of evoked responses before and after 10 min bath application of 10 mM BIC (black bars) 473 nm light pulses. **e**, Group data representing mean ± S.E.M of evoked responses before and after 10 min bath application of

10 mM BIC (N = 5 cells from N = 5 mice, t=4.369 df=4.014, P = 0.0119 using unpaired two-tailed Student's t-Test). **f**, Group data representing mean ± S.E.M of paired-pulse ratio of optogenetically-induced IPSCs from TRN recorded cells before and after bath application of 10 mM bicuculine (N = 5 cells from N = 5 mice, t=0.0838 df=8, P = 0.935) using unpaired two-tailed Student's t-Test.

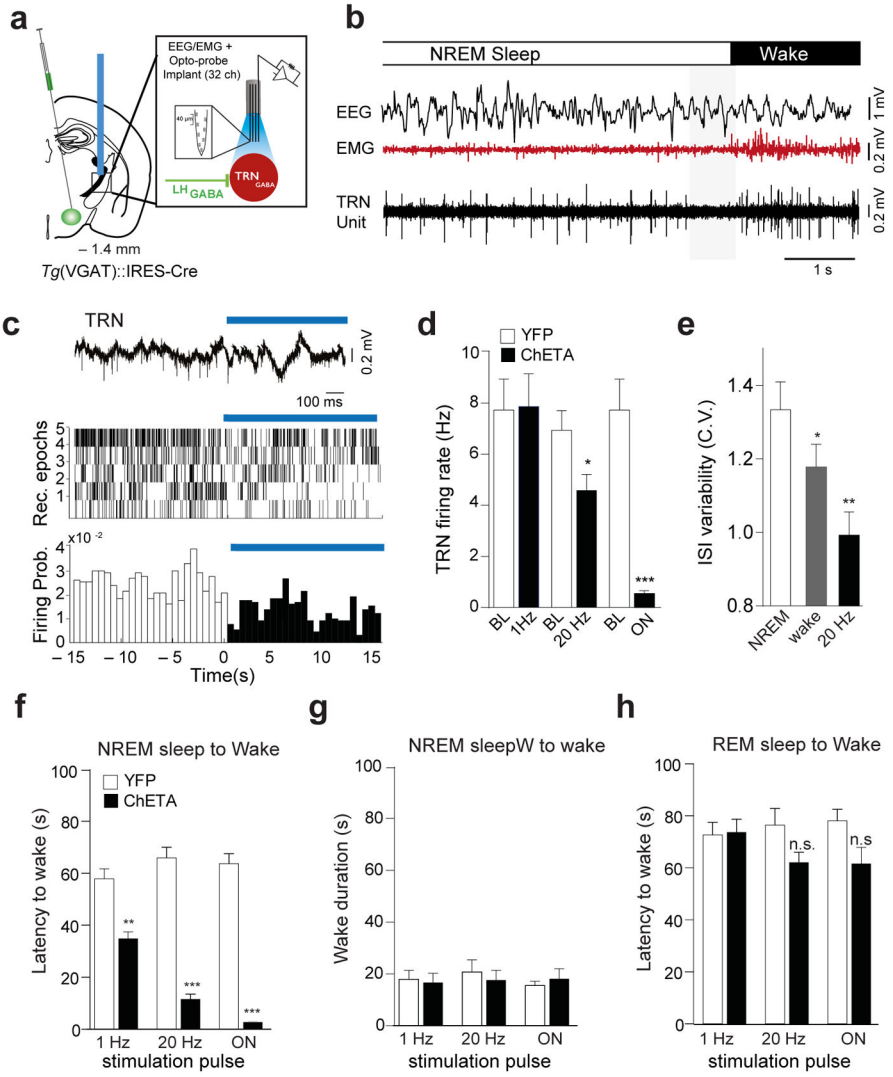

Figure 3. Optogenetic stimulation of LH_{GABA}-TRN circuit induces rapid arousal

a, Schematic of the *in vivo* recording set up. **b**, Representative traces showing EEG/EMG/TRN Unit recording during the a spontaneous NREM sleep-to-wake transition in a freely-moving mouse (EEG/EMG traces from 19 recordings, N=3 mice). Note the transient period of TRN cell quiescence preceding behavioral transition (shaded box). TRN units were consistently recorded in 3 separate sets of experiments. **c**, Representative signal trace of a TRN unit (wide band) before and after the onset of optical activation of LH_{GABA} terminals (*top*). Rastergrams of 5 representative TRN cells (N=2 mice) (*middle;* of 70 recorded TRN cells) and their firing probability (*bottom*) before and after the optical stimulation. Blue bar show the optical stimulation (473 nm). **d**, Average firing rates ± S.E.M of TRN neurons during baseline and upon optical stimulation of LH_{GABA}-TRN projections at different frequencies (1 Hz: N = 17, 20 Hz: N = 57, 2-s continuous illumination: N = 17). Optical stimulation led to a frequency-dependent (P 9.4 $\times 10^{-16}$, F(3,3)=3.28, one-way ANOVA followed by Bonfferoni post-hoc test) decrease in the firing rate. Statistical significance was given to values *, $P < 0.05$, ***, $P < 0.0001$, Student t-tests with α adjusted

for multiple comparisons. **e,** Coefficient of interspike intervals variation (CV) of TRN cells across NREM sleep and wake states (Kruskal Wallis test, $P=3.52\times10^{-9}$) and upon optogenetic activation of LH_{GABA}-TRN circuit at 20 Hz ($P=0.0082$). **f**, Mean latencies of NREM (*left*) and REM (*right*) sleep-to-wake transitions upon optogenetic stimulation at 1 Hz (ChETA $N=7$, YFP $N=5$, t=5.21 df=10, $P=0.0004$, unpaired two-tailed Student's t-Test); 20 Hz (ChETA $N=7$, YFP $N=5$, t=13.2 df=10, $P=0.00001$ unpaired two-tailed Student's t-Test or 1-s continuous (ChETA $N=7$, YFP $N=5$, t=19.1 df=10, $P=0.0001$, unpaired two-tailed Student's t-Test) illumination in control (white) and ChETA-EYFP (black) mice. Data analysis based on > 10 stimulations per frequency and per animal (*N*). statistical significance was given to values **, $P<0.001$, ***, $P<0.0001$. **g**, Mean duration ± S.E.M of optogenetically-induced wake episode upon optical stimulation at 1 Hz (ChETA, $N=7$, YFP, $N=6$, t=0.253 df=11, $P=0.804$), 20 Hz (ChETA, $N=7$, YFP, $N=6$, t=0.827 df=11, $P=0.4259$), and 1s-continuous illumination ($N=7$, YFP, $N=6$, t=0.568 df=11, $P=0.5815$ using unpaired two-tailed Student's t-Test). **h**, Mean latencies ± S.E.M of REM sleep to wake transition upon optical at 1Hz stimulation (ChETA $N=4$, YFP $N=5$; t=0.139 df=10, $P=0.891$); 20 Hz (ChETA $N=4$, YFP, $N=5$, t=2.03 df=10, $P=0.069$); and 1s-continuous illumination (ChETA, $N=4$, YFP, $N=5$, t=1.93 df=10, $P=0.0786$) in control (white) and ChETA-EYFP (black) mice, respectively. Data analysis based on > 10 stimulations per frequency and per animal (*N*). **, $P<0.001$, ***, $P<0.0001$

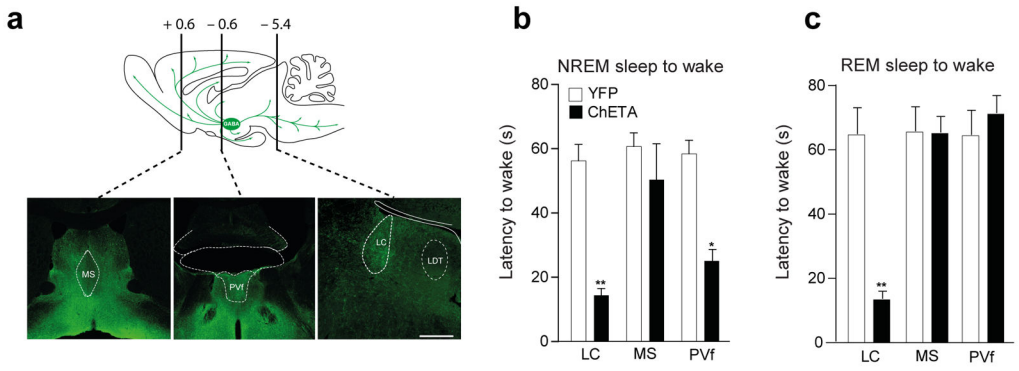

Figure 4. LH_{GABA} neurons control arousal trough multiple pathways

a, Schematic of sagittal section showing LH_{GABA} neuron projections in the rodent brain. *Bottom*, representative photomicrograph of coronal brain sectionsshowing EYFP-expressing axons from LH_{GABA} cells in the medial septum (MS), periventricular thalamus (PvT) and the locus coeruleus (LC). Representative images from repeated experiment (> 15 sections from $N = 4$ transduced mice). Scale bar: 500 μm. **b**, **c**, Mean latencies ± S.E.M of NREM (*left*) and REM (*right*) sleep-to-wake transitions upon 1-s optogenetic stimulation in control (white) and ChETA-EYFP (blue) animals (Data analysis based on > 10 stimulations per frequency and per animal $N = 4$ in each group, F(5,16= 0.479, P=0.029). *, $P < 0.05$; **, $P < 0.001$ using one-way ANOVA followed by multiple comparisons Bonfferoni post-hoc test.

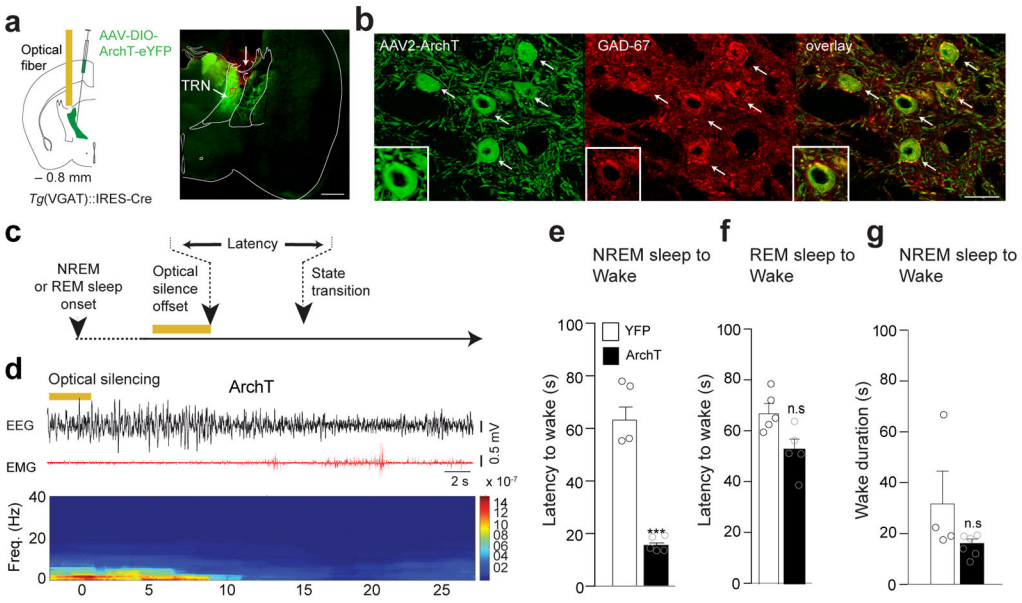

Figure 5. LH_{GABA}-TRN induced arousal is due to direct inhibition of TRN cells

a, Shematic (left) of the genetic targeting of TRN_{GABA} neurons. AAVdj-DIO-ArchT-YFP or AAVdj-DIO-YFP were infused into the TRN of VGAT::Cre animals. Representative photomicrograph (right) of a coronal hemi-section showing ArchT-YFP expressing TRN cells in the anterior TRN Arrow indicates the injection tract. Scale bar, 500 μm. **b**, Representative photomicrograph magnification of the red box in panel (**a**). Scale bar, 50 μm. White arrows on the photomicrographs indicate ArchT-EYFP expressing TRN cells (green) positive for GAD-67^{+} (red) and merge images (*right*). Higher photomicrograph magnification shows colocalisation of EYFP and GAD-67 immunolabelling. Representative images from repeated experiment (> 15 sections from $N = 5$ transduced mice in each group). **c,** Schematic of the experimental timeline. **d,** Representative EEG/EMG traces and the corresponding heat map EEG power spectrum illustrating behavioral response to optogenetic silencing (bilateral 5-s continuous illumination, indicated by horizontal yellow bars; 593 *nm*) during NREM sleep. Note the decrease of the amplitude of low frequency (< 4Hz) oscillations and the EMG tone at NREM-to-Wake transition. **e, f**, Mean latencies ± S.E.M wake transitions during NREM (**e**) (ArchT $N = 6$, YFP $N = 4$, t=8.54 df=8, p=0.0001) and REM (**f**) sleep (ArchT $N = 6$, YFP $N = 5$, t=1.79 df=9, p=0.1073) after a single 5s-continuous illumination. Data analysis based on > 10 stimulations per frequency, per state and per animal (N). ***, $P < 0.0001$; n.s., $P = 107$ using unpaired two-tailed Student's t-Test. **g,** Mean wake duration ± S.E.M upon optogenetic silencing of TRN cells during NREM sleep in control (*white)* and ArchT (*black)* mice(ArchT $N = 6$, *YFP* N=4, t=1.49 df=*8, P*=0.1753). n.s., $P = 0.184$ using a two-tailed Student's *t*-Test.

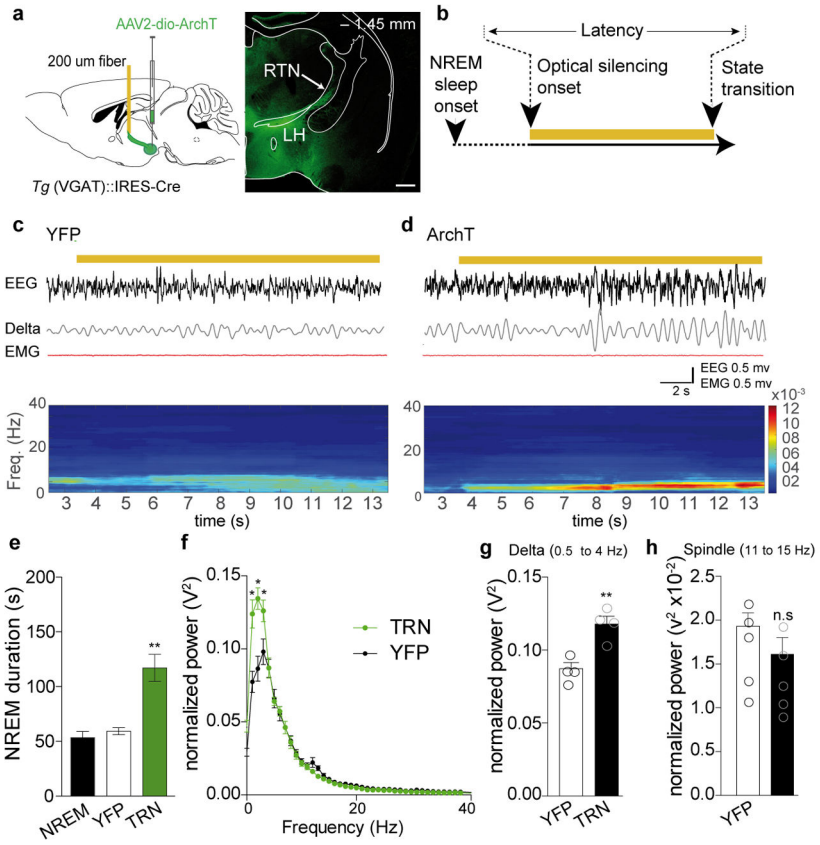

Figure 6. Inhibition LH_{GABA} projections to the anterior TRN during NREM causes increase in total length of NREM sleep compare to control conditions

a, Schematic of experimental preparation (left). AAV2-DIO-ArchT-EYFP and AAV2-DIO-EYFP (control) were infused in the LH (AP: −1.45 mm) of Tg(VGAT)::IRES-Cre animals. Bilateral fibers were implanted at the level of the anterior TRN (AP: −0.85 mm). *Right*, Photomicrographs of a coronal brain hemisection showing EYFP labelling of LH cell bodies targeting and projections to the TRN. **b**, Schematic of the experimental timeline. Light was delivered continuously 10 s after of the onset of a stable NREM sleep and terminated at the next transition (REM or wake). Representative images from repeated experiment (> 10 sections from n = 4 transduced mice in each group). **c, d,** Representative EEG/EMG traces and EEG heat map of control (EYFP, ***c***) and ArchT-EYFP (***d***) animals showing changes in the EEG (top) delta (0.5–4 Hz) oscillation (middle), EMG and correspondent heat map EEG power spectrum (bottom) in response to local optical silencing (yellow bar, 593 nm) of LH_{GABA}-TRN circuit during NREM sleep. **e**, Mean duration ± S.E.M of NREM sleep episodes during baseline (*left, grey bar*), and during optogenetic inhibition in control (white) and ArchT-EYFP (black) mice (N = 4 per group; Data analysis based on > 10 stimulations per frequency and per animal during NREM sleep episode. T(3,12)=21.45, P=0.00001) **, P < 0.01 using one-way multiple ANOVA followed by Bonfferoni post-hoc test. **f,** Mean ± S.E.M average of normalized spectral power distribution of relative cortical EEG power density in control animals (grey trace) and ArchT-EYFP (black trace) animals (n = 5 NREM episodes per animal. n=4 animals per group, t=0.239 df=484, P=0.811) upon optical

silencing. *, $P < 0.05$ using unpaired two-tailed Student's *t*-Test between control and ArchT animals. **g,** Quantification of the relative cortical EEG power of delta (n=4 mice per condition, $N = 5$ NREM episodes per animal, t=4.42, P=0.0052, unpaired two-tailed Student's t-Test); **, $P < 0.05$) (***h***) and spindle frequencies upon optogenetic silencing of EYFP and ArchT-EYFP animals during NREM sleep ($N = 4$ mice per condition, $N = 5$ NREM episodes per animal, t=1.16, P=0.28); *n.s.,* $P < 0.28$ using unpaired two-tailed Student's *t*-Test.

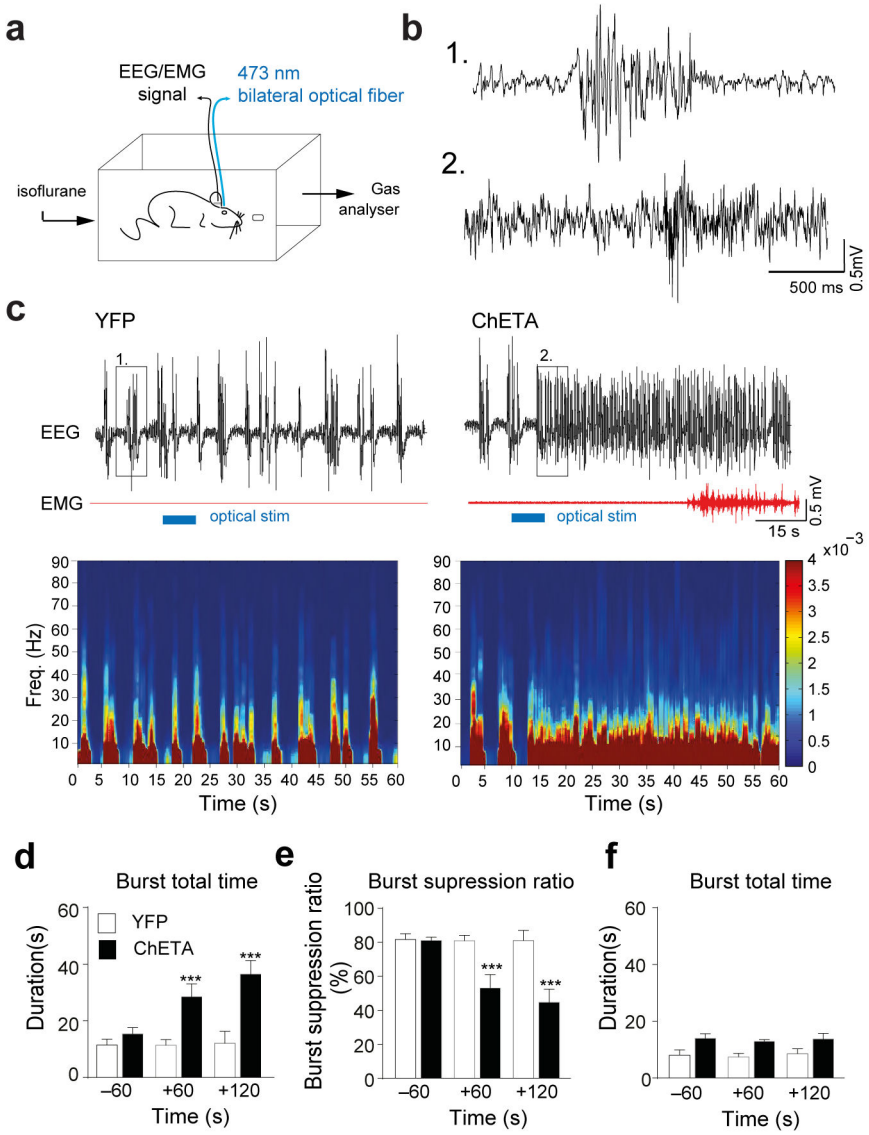

Figure 7. Activation of the LH_{GABA}-TRN circuits induced cortical arousal and emergence from anesthesia

a, Shematic representation of the *in vivo* polysomnographic recording set up in anesthetic chamber. **b**, Higher time resolution of of EEG traces shown in (c) depicted by the boxes (1) for control condition and (2) for ChETA-EYFP positive animals after 5 sec light stimulation of the TRN. These illustrate changes at the level of cortical EEG of burst-suppression ration after stimulation during anesthesia (1–1.2 % isoflurane). **c**, Representative EEG/EMG recordings and heat map EEG power spectrum before, during and after single 5-s optical stimulation (horizontal blue bars) in EYFP (*left*) and ChETA-YFP (*right*) animals during deep anaesthesia. Note the muscle tone that occured in ChETA-YFP (2 out of 5 animals). **d**, Mean duration ± S.E.M of burst total time (**e**), burst suppression ratio and (**f**), and burst total time duration, before and after bilateral optical stimulation delivered during the EEG burst in control (white) *N* = and ChETA-EYFP (black), (*N* = 4 mice, 3 repetitions per animal). **f**, Mean duration ± S.E.M of burst total time before and after bilateral optical stimulation

delivered during isoelectric period in control (white) and ChETA-EYFP (black) ($N = 4$ mice, 3 repetitions per animal). ***, $P < 0.0001$ using a two-tailed Student's t-Test.